Results in Chemistry 8 (2024) 101604

Contents lists available at ScienceDirect

Results in Chemistry

journal homepage: www.sciencedirect.com/journal/results-in-chemistry

# Fabrication of a novel MOF template-derived $ZnCo_2O_4$ composite for the non-enzymatic electrochemical detection of glucose

K. Divyarani [a], S. Sreenivasa [a,*], Sandeep Kumar [b], Anjana Vinod [b], Fahd Alharethy [c], Byong-Hun Jeon [d,*], V.S. Anusuya Devi [e,*], Praveen Martis [f], L. Parashuram [b,*]

[a] Department of Studies and Research in Chemistry, Tumkur University, Tumkur 572101, India
[b] Department of Chemistry, Nitte Meenakshi Institute of Technology, Yelahanka, Bangalore 560064 India
[c] Department of Chemistry, College of Science, King Saud University, Riyadh 11451, Saudi Arabia
[d] Department of Earth Resources and Environmental Engineering, Hanyang University, 2226 Wangsimni-ro, Seongdong-gu, Seoul 04763, South Korea
[e] Department of Chemistry, New Horizon College of Engineering, Outer Ring Road, Bangalore 560103, India
[f] Loyola Centre for Research and Innovation, St Aloysius Deemed to be University, Light House Hill Road, Mangalore, Karnataka 575003, India

ARTICLE INFO

*Keywords:*
Glucose Sensor
Non-enzymatic
MOF-templated

ABSTRACT

Glucose detection is one of the frequently occurring research due to increased cases of diabetes and the need for continuous monitoring of glucose. MOF template-derived nanocomposites have shown their potential in the field of sensors to address the shortcomings due to selectivity and sensitivity of the present-day sensors. A novel MOF template-derived $ZnCo_2O_4$ Composite ($ZnCo_2O_4$@MOF) sensing was designed and prepared in this study, and it was employed as an electrochemical sensor for the non-enzymatic detection of glucose with good selectivity and stability. The electrochemical characteristics of the present sensor were evaluated using a cyclic voltammetry (CV), differential pulse voltammetry (DPV), electrochemical impedance spectroscopy (EIS), and amperometry i-t. The template-mediated process and the synergism between the metallic components in the electrocatalyst have provided high electroactive surface area, electrolyte diffusion, and excellent stability that promote electron transfer and enhance the response current. With a wide linear range (0.1 – 100 μM), and 24.8 nM of low detection limit (S/N = 3). The constructed non-enzymatic biosensor exhibited long-term stability and remarkable reproducibility. Furthermore, the $ZnCo_2O_4$@MOF composite-modified electrode showed an excellent anti-interference ability against the common molecules that interfere during the detection of glucose.

## Introduction

Diabetes is a chronic health disorder, that is marked by the consistent inability of the body to appropriately manage the glucose level in the blood [1]. Rigorous monitoring of blood glucose levels is significant for managing diabetes and to reduce the problems associated with it. Major complications like diabetic nephropathy, diabetic retinopathy, cardiovascular diseases, stroke, and limb amputation have led to reduced life expectancy and increased morbidity [2]. The devastatingly increasing number of diabetes-related diseases in India has become a huge challenge. These problems are alarming and need to be critically addressed with a proper healthcare system and proper monitoring equipment. The socioeconomic burden on patients has caused delayed and missed diagnoses. Hence there is an urgent need to develop a reliable glucose monitoring system that is cost-effective and has high sensitivity and selectivity [3,4]. See Fig. 1.

Major technological advances and scientific innovations for developing non-invasive systems to monitor glucose have been witnessed in the last decade [5–7]. Glucose can be monitored by switching over to electrochemical sensing techniques which are painless and non-invasive by avoiding afflicting finger-pricking blood sampling techniques [8–13]. Instead, analysis is carried out by exploiting external assays of body fluids such as tears, saliva, and breath. Even though great progress has been accomplished in the field of glucose biosensing, still it suffers from serious flaws. Enzyme-based glucose sensors struggle with the problems of pH, temperature, enzyme denaturation, complex process of enzyme purification, low stability, and ionic strength. Non-enzymatic glucose sensing is of clinical and industrial relevance as it relies directly on the

* Corresponding authors at: Department of Chemistry, Nitte Meenakshi Institute of Technology, Yelahanka, Bangalore 560064, India.
*E-mail addresses:* drsreenivasa@yahoo.co.in (S. Sreenivasa), bhjeon@hanyang.ac.kr (B.-H. Jeon), anukmp@gmail.com (V.S.A. Devi), ramacademy1990@gmail.com (L. Parashuram).

https://doi.org/10.1016/j.rechem.2024.101604
Received 28 February 2024; Accepted 13 June 2024
Available online 14 June 2024

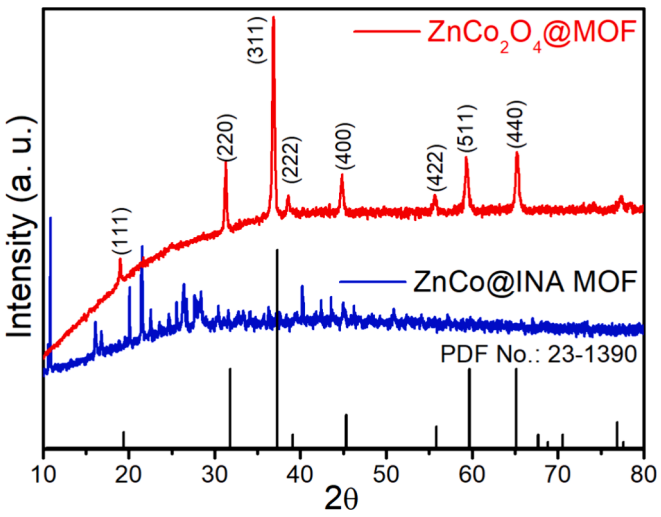


**Fig. 1.** XRD patterns of ZnCo@INA MOF and $ZnCo_2O_4$@MOF. The respective peaks are indexed to the standard JCPDS No. 23–1390.

oxidation or reduction of glucose. It is a rapid, stable, and cost-effective technique. But it also has some limitations which include surface poisoning, lower selectivity, inactivity, and less sensitivity at neutral pH.

MOFs are versatile materials that serve as both precursors and templates in the synthesis of cost-effective nanomaterials including metal oxides, porous carbon, metal sulfides, and layered double hydroxides [14,15]. Due to their well-dispersibility, hollow architectures, and easy tunability, they are widely used in the field of electrochemical sensing [16–18]. Due to the unique advantages of porous carbon materials which have huge pores, and higher chemical and mechanical resilience, these materials have potential in gas sensing, electrochemical sensing, and energy conversion. The activity of these materials relies on the preparation method and is crucial for multiverse applications. When the materials are prepared by direct carbonization of the precursors, it may lead to porous carbons having larger sizes with disordered structures and may limit the selective diffusion of molecules or analytes during sensing. Hence to deal with this limitation, a template carbonization strategy is useful since it controls the pore architectures along with the desired size.

The nanostructures of ZnO and other metal oxide composites are suitable candidates due to their good thermal stability, higher electron mobility, and large exciton binding energy [19–21]. The ZnO shows cubic zinc blende phase and hexagonal wurtzite phases. Among them, wurtzite is stable to humidity and can have different morphologies. It has polar surfaces consisting of $Zn^{2+}$ and $O^{2-}$, having tetrahedral coordination, and hence is used in sensing devices and actuators [22,23]. The zinc oxide has higher optical transparency and hence can be used in the preparation of transparent conductive films. Along with that, the isoelectric point of ZnO is 9.5, this allows immobilization of elements having low isoelectric points by electrostatic contact. The fascinating features of $Co_3O_4$ such as electrocatalytic activity, its affordability, and its efficiency have attracted their interest in the field of sensing [24–29]. It has a close-packed cubic distribution of oxides where Co(II) and Co (III) occupy tetrahedral and octahedral sites. On the same lines $Co_3O_4$ has higher electrochemical activity and is a p-type semiconductor. Because of its higher electrochemical stability and high activity, it is used in the detection of hydrogen peroxide and glucose. The presence of zinc, which has higher electron abundance in combination with cobalt results in a nanocomposite that is highly electron-rich and hence becomes an appealing material for sensor application [30]. In this study, we have reported MOF template-mediated synthesis of $ZnCo_2O_4$ for non-enzymatic glucose sensing. The fabricated $ZnCo_2O_4$@MOF were examined for their crystal structure and morphological features by XRD and FESEM, respectively. The $ZnCo_2O_4$@MOF was characterized by XPS and EDS to determine its composition. This $ZnCo_2O_4$@MOF showed high sensitivity and selectivity for glucose detection. Good reproducibility and higher recovery rates further encourage the use of $ZnCo_2O_4$@MOF in the field of biomedical applications. Herin, we demonstrate a novel $ZnCo_2O_4$@MOF-based non-enzymatic glucose sensor for rapid determination of glucose in natural perspiration. The novel template-assisted preparation of $ZnCo_2O_4$@MOF has significantly improved the electroactive surface area. The proposed non-enzymatic sensor was examined for the quantitative estimation of glucose in human blood serum samples at physiological pH, demonstrating its real-time application. The novelty of the sensor lies in the microelectrode system with minimal electrocatalyst, improved surface area, rapid current response, outstanding catalytic efficiency of the microsensor, wide linear range, lower detection limit, and interference-free detection of glucose in spiked as well as the real blood samples makes it a robust electrochemical platform for the quantification of glucose.

## Experimental

### *Reagents and materials*

Cobalt (II) chloride hexahydrate ($CoCl_2{\cdot}6H_2O$), Zinc nitrate hexahydrate ($Zn(NO_3)_2{\cdot}6H_2O$), isonicotinic acid ($C_6H_5NO_2$), graphite flakes, D-glucose (D-$C_6H_{12}O_6$), ascorbic acid (AA), sodium chloride (NaCl), uric acid (UA), dopamine (DA) were purchased from Sigma-Aldrich chemical company. DMF, $H_2SO_4$, and HCl were procured from Qualigen's fine chemicals. Ethylene glycol, hydrogen peroxide, and ethanol were purchased from SDFCL. Deionized water was used to prepare the aqueous solutions.

### *Preparation of $ZnCo_2O_4$@MOF*

Briefly, 0.5948 g of $CoCl_2{\cdot}6H_2O$ (0.0025 M) was dissolved in a solvent system containing 25 ml DMF and 10 ml ethylene glycol. Afterward, 0.3718 g of Zn $(NO_3)_2{\cdot}6H_2O$ (0.00125 M) and 0.6155 g of isonicotinic acid (0.005 M) were added to the above solution. The obtained pink solution was transferred to a Teflon-lined stainless steel autoclave and then kept in a hot air oven maintained at 150 °C for 12 h. After that, the solution was subjected to centrifugation at 5000 rpm for 15 min. Then, it was washed with ethanol three times. The obtained pink solid was dried in a hot air oven maintained at 70 °C and further calcinated at 500 °C to get the $ZnCo_2O_4$@MOF.

### *Preparation of $ZnCo_2O_4$@MOF modified CPE electrode*

A carbon paste-loaded diabetic syringe electrode (carbon paste electrode-CPE) was polished successively with 1.00 μM, 0.30 μM, and 0.05 μM alumina slurry to get a mirror-like surface. The surface was cleaned by ultrasonicating the CPE in distilled water followed by ethanol. $ZnCo_2O_4$@MOF electrocatalyst was suspended in DMF (1 ml) and sonicated for 10 min to get the homogeneous suspension, then 5 μL of the $ZnCo_2O_4$@MOF suspension was dropped onto the surface of CPE to form a thin film and dried overnight.

### *Electrochemical studies*

Electrochemical Experiments for the application of glucose sensing were carried out on a CHI 660E instrument equipped with the conventional three-electrode system. The fabricated $ZnCo_2O_4$@MOF on a carbon paste electrode was used as a working electrode, platinum wire as the counter electrode, and the Ag/AgCl electrode was used as a reference electrode. KCl/$NH_4$OH-$NH_4$Cl, pH = 10 suitably adjusted with NaOH is used as an electrolyte system. The electrocatalytic activity of the $ZnCo_2O_4$@MOF/CPE towards glucose was examined using CVs run from − 0.8 V to + 0.8 V at a scan rate of 100 mV·$s^{-1}$ ($NH_4$OH-$NH_4$Cl, NaOH, pH = 10) as an electrolyte. EIS was performed at frequencies in 5

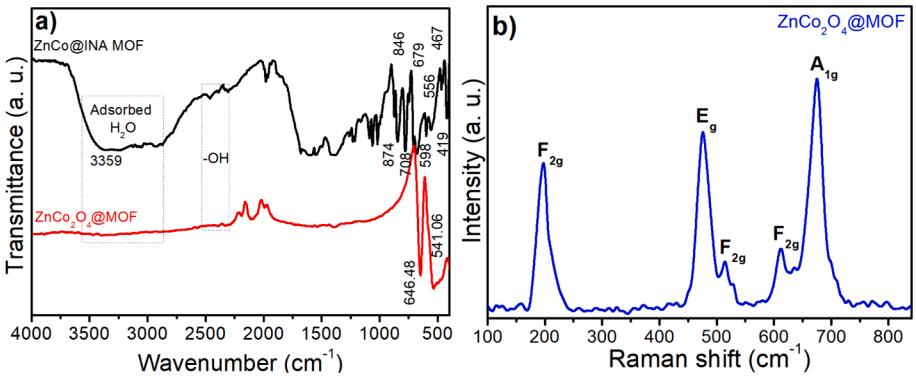


**Fig. 2.** A) ftir spectra of ZnCo@INA MOF and $ZnCo_2O_4$@MOF recorded in KBr. b) Raman spectrum of $ZnCo_2O_4$@MOF electrocatalysts.

mM potassium ferricyanide from 0.01 Hz to 100 kHz with 10 mV amplitude to understand the electron transfer properties. The amperometric response of the modified electrode for glucose detection was measured by successively adding aqueous glucose solution into the magnetically stirred electrolyte at an applied potential of −0.4 V vs. Ag/AgCl. Before a subsequent determination, the remaining glucose was removed from the working electrode by several cycles in the fresh electrolyteselectrolytes.

*Preparation of human blood serum*

The human blood samples collected were placed in a water bath maintained at 40 °C for 12 min. Then it was centrifugated by a centrifuge machine at 4000 rpm for 5 min. The obtained supernatant was collected and stored in a lab refrigerator maintained at –10 °C to 0 °C.

*Characterization*

XRD was performed to determine crystalline phase purity on the Rigaku Smart lab, Japan (CuKα radiation source, $\lambda = 1.5406$ Å, $2\theta = 10 - 80°$ the scanning rate was 5°/min, and the temperature was 25 °C). The composition and morphology were studied by FESEM. Dried samples were glued on the sample stage with conductive tape with the observation side facing up. Finally, high-energy incident electrons were used on the Hitachi model: S-3400 N. EDS was performed by Peltier cooled X-ray head from Thermo, USA. TEM images were recorded by JEOL, 2100F model, The high-resolution TEM micrographs were acquired on a Cs-probe corrected Jeol 2100F Transmission Electron Microscope operated at 200 kV. The images were recorded on an Ultrascan CCD camera upon 1 s exposure for each image. Thermo Nicolet Model: 6700 instrument was used to record FTIR by dispersing samples in KBr (400 to 4000 $cm^{-1}$) with an average of 32 scans and a resolution of 2 $cm^{-1}$. Elemental analysis was performed on a Thermoscientific NEXA surface analyzer.

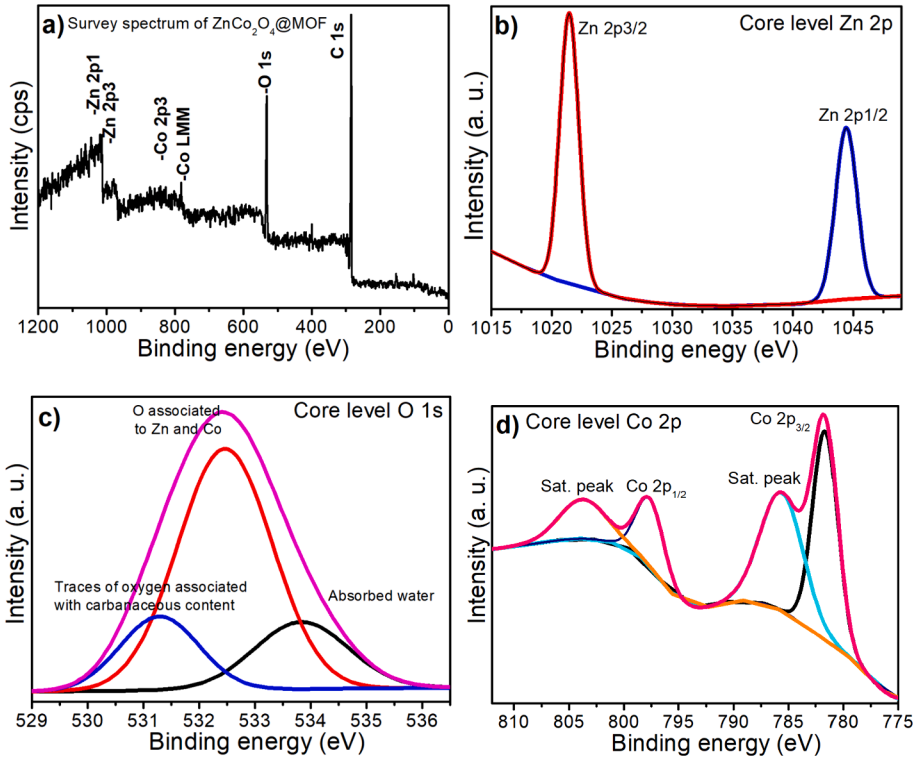


**Fig. 3.** XPS spectra of $ZnCo_2O_4$@MOF a) Survey spectrum indicating the presence of Zn, Co, and O; core-level spectrum of b) Zn showing Zn $2p_{3/2}$ and $2p_{1/2}$, c) showing O1s associated under different environment and d) Cobalt showing the presence of Co in variable oxidation states.

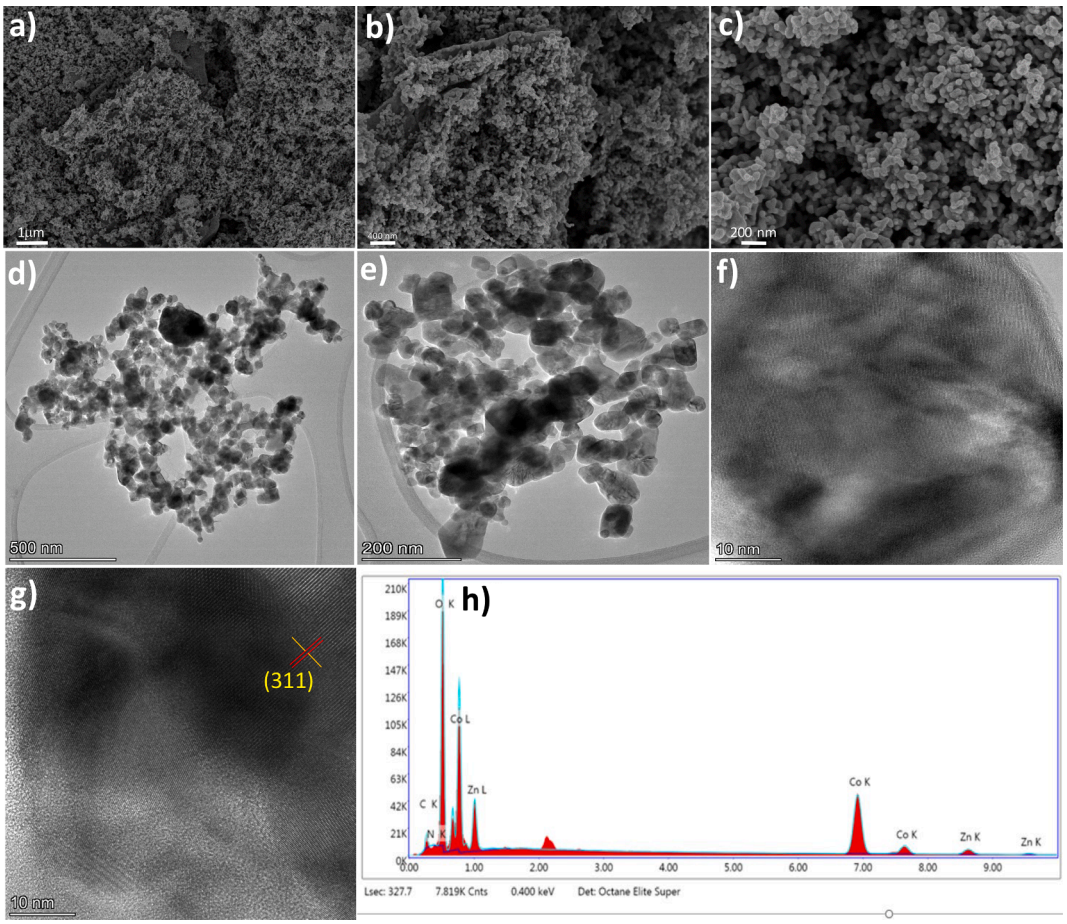


**Fig. 4.** FESEM micrographs a-c (Magnification from 1 mμ – 200 nm); TEM images d and e(Magnification from 500 nm – 10 nm); f) HRTEM images recorded at 10 nm indicating the lattice fringe (311) in the inset. and g) EDX spectrum of $ZnCo_2O_4$@MOF, showing the presence of Zn, Co, and O.

## Results and discussions

The crystal structure and phase purity were determined by examining the XRD pattern of ZnCo@INA MOF and $ZnCo_2O_4$@MOF. The diffraction peaks corresponding to the ZnCo@INA MOF are in very good agreement with the previous literature. For $ZnCo_2O_4$@MOF the peaks appeared at 19.14°, 31.34°, 37.01°, 38.71°, 44.9°, 55.72°, 59.49°, and 65.33°, which accords with the plane indexed to (111), (220), (311), (222), (400), (422), (511), and (440), respectively. This data is in very good correlation with the XRD of the standard with JCPDS card number 23–1390. The CoO crystallite phase was confirmed by the distinct diffraction peaks attributed to the presence of $ZnCo_2O_4$. The primary diffraction peaks of ZnCo@INA MOF are completely different from the XRD peaks of $ZnCo_2O_4$@MOF. This demonstrates the successful formation of MOF template-mediated $ZnCo_2O_4$ [31,32].

The adsorption peaks range from 1656 − 1590 $cm^{-1}$ are associated with asymmetric vibrations of the carboxylate functional group and the peaks situated in the range of 1400 − 1550 $cm^{-1}$ correspond to symmetric carboxylate functional group in the case of ZnCo@INA MOF. This implies the coordination of $Zn^{2+}$ ions with the isonicotinic acid ligand. The peaks arising in the range of 690 − 770 $cm^{-1}$ are attributed to vibrations of metal–oxygen bonds in the synthesized material, as well as peaks found below 550 $cm^{-1}$ are due to the existence of ZnO in the prepared MOF. In the case of $ZnCo_2O_4$@MOF, all the peaks corresponding to the organic groups have completely disappeared, this is attributed to the removal of all organic groups upon high-temperature treatment to yield $ZnCo_2O_4$. Two prominent peaks were observed in the case of $ZnCo_2O_4$@MOF at 541.06 $cm^{-1}$ and 646.48 $cm^{-1}$, these peaks indicate the formation of direct metal–oxygen bonds between Zn-O, Co-O, and metal–oxygen-metal type of vibrations, respectively [33,34]. The Raman spectrum of $ZnCo_2O_4$@MOF is shown in Fig. 2b). Five fundamental Raman modes were observed, which resemble F2g (194.3 $cm^{-1}$), Eg (475.4 $cm^{-1}$), F2g (514.7 $cm^{-1}$), F2g (612.9 $cm^{-1}$), and A1g (676.6 $cm^{-1}$) of $ZnCo_2O_4$ phase. Further Raman spectroscopy analysis confirmed the formation of high-quality $ZnCo_2O_4$@MOF.

The chemical environment and surface characteristics of $ZnCo_2O_4$@MOF were arbitrated by XPS. The elements Co, Zn, and O were visualized in the survey spectrum (Fig. 3a). To have clear information from the XPS spectra, the core level peaks obtained for cobalt, zinc, and oxygen were deconvoluted. The Zn XPS spectra were visualized by the peaks located at 1021.5 eV and 1044.5 eV corresponding to Zn $2p_{3/2}$ and Zn $2p_{1/2}$ (Fig. 3b). The presence of zinc in its ionic state is demonstrated by the energy of split separation between $Zn2p_{1/2}$ and $Zn2p_{3/2}$. The presence of Zn-O bonds was confirmed from the curefitting analysis applied to $Zn2p_{3/2}$. Two characteristic peaks that arise for cobalt at 781.8 eV and 797.9 eV are ascribed to Co $2p_{3/2}$ and Co $2p_{1/2}$ respectively (Fig. 3c). These peaks along with the presence of satellite peaks corresponding to Co $2p_{3/2}$ and Co $2p_{1/2}$ have substantiated the existence of mixed oxidation states of cobalt i.e. + 2 and + 3 [35]. The oxygen peak was deconvoluted further into three peaks each corresponding to the oxygen associated with the metal ions zinc and cobalt. The presence of oxygen in the form of hydration and a trace quantity of oxygen present in the form of organic functionality, that originates from the precursor isonicotinic acid ligand (Fig. 3d). The Zn: Co atomic ratio was calculated, by computing the area under the respective peaks divided by the RSF factor to the sum area of all the elements divided by their RSF. The ratio Zn: Co was found to be 1:1.934 based on the XPS band area, which is close to the designed ratio of $ZnCo_2O_4$ (Zn: Co =

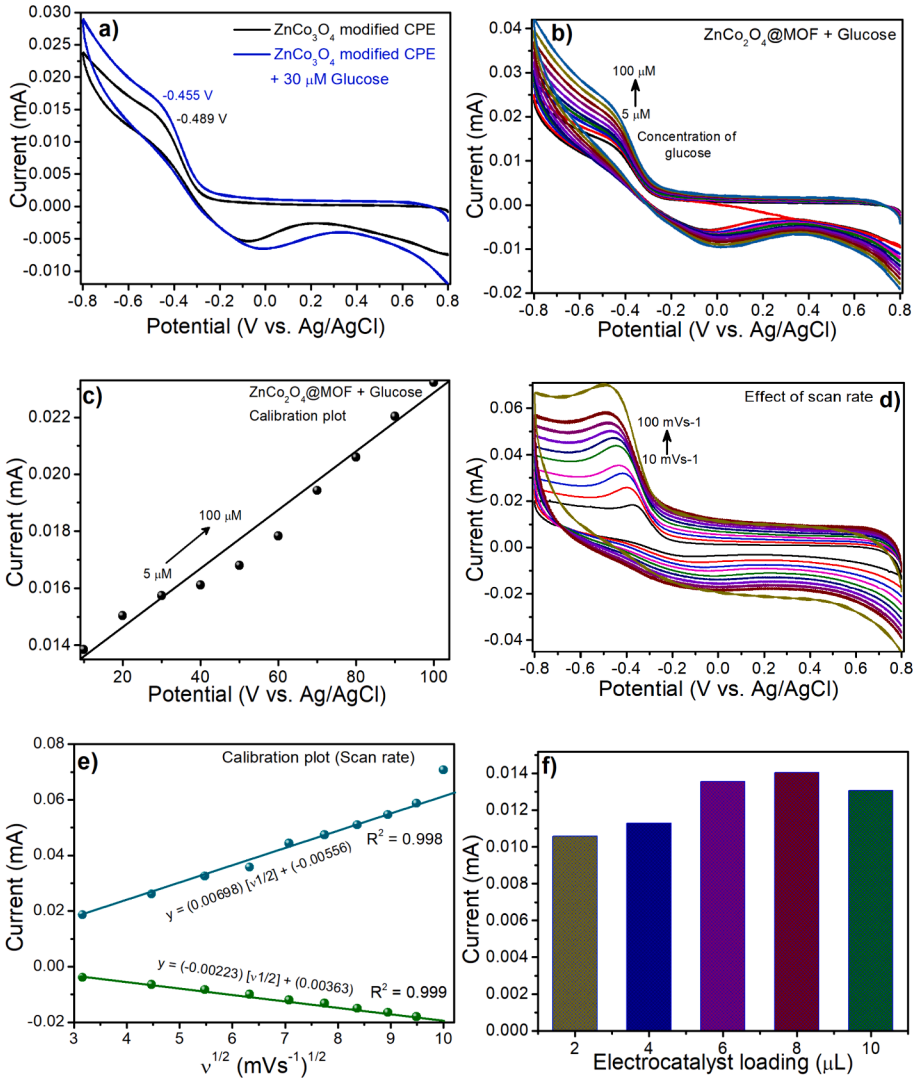


**Fig. 5.** A) the cyclic voltammograms in the absence and presence of 30 μM glucose at ZnCo2O4@MOF/CPE in 0.1 M KCl medium; b) CV response with the variation of concentration of glucose (5 μM – 100 μM, SR = 100 $mVs^{-1}$; c) corresponding calibration plot in ($NH_3$–$NH_4Cl$, NaOH, pH≈10) at $ZnCo_2O_4$@MOF/CPE at a scan rate of 100 $mVs^{-1}$ d) Effect of scan rate on the current response, showing both anodic and cathodic response (10 – 100 $mVs^{-1}$) e) corresponding calibration plot and f) Effect of electrocatalyst loading on the current response (2 – 10 μL of $ZnCo_2O_4$@MOF suspension on CPE, SR = 100 $mVs^{-1}$, pH≈10).

1:1.98). Further, the values are reverified XPSPEAK and found to be in good agreement.

The microstructures of the fabricated $ZnCo_2O_4$@MOF were explored by FESEM. The FESEM shows the pile of $ZnCo_2O_4$@MOF nanoparticles uniformly distributed in the entire structure. These components gave the intricate pattern for $ZnCo_2O_4$@MOF which are highly porous with several cracks [36,37]. The obtained images of the prepared $ZnCo_2O_4$@MOF reveal that the particles show uniform stone-gravel structures with diameters averaging to < 30 nm (Fig. 4a–c). The TEM image of the synthesized $ZnCo_2O_4$@MOF is shown in Fig. 4c and e). The assembly of ZnCo@MOF on the surface is revealed from the TEM images. Further, the interplanar fringes were identified in the HRTEM images (Figures f and g). Also, it can be noted that the formation of $ZnCo_2O_4$@MOF stone-gravel structures with highly restrained particle aggregation thereby increasing electrochemical stability [38,39]. The semi-quantitative analysis from the EDS mapping results shows the weight percentages of cobalt, zinc, carbon, oxygen, and nitrogen. The results are listed in Fig. 4h), the composition mapping of $ZnCo_2O_4$@-MOF is in good agreement with that of the experimental composition used for the preparation of $ZnCo_2O_4$@MOF.

*CV measurements*

The CV responses of $ZnCo_2O_4$@MOF/CPE were performed in a solution containing 0.1 M KCl at 100 $mVs^{-1}$ scan rate in the presence and absence of glucose as displayed in Fig. 5a). The CV curve of $ZnCo_2O_4$@MOF was comprised of redox peaks, this would be attributed to the reversible oxidation and reduction of cobalt present in the composite, which further ascertains the existence of dual oxidation states of cobalt. It was clear from the CV that the oxidation peak positioned at −0.489 V has noticeably shifted to −0.455 V with an increase in the current response upon the addition of 30 μM of glucose. This demonstrates that the electrode is sensitive and shows a response towards glucose. Getting motivated from this initial observation, we have explored the current response of the sensor with variable concentrations of glucose from 5 μM-100 μM. As obvious the current response has increased linearly with an increase in the concentration of the glucose following the linear regression equation $i_a = (1.02184e^{-7})$ [glucose] + $(1.24443e^{-5})$ with $R^2 = 0.987$ (Fig. 5c). The electroactive surface area of unmodified CPE and $ZnCo_2O_4$@MOF/CPE was computed by performing the CV tests at varied scan rates. Fig. 5d shows the CV redox current of $ZnCo_2O_4$@MOF/CPE at various scan rates of 10–100 $mVs^{-1}$ in

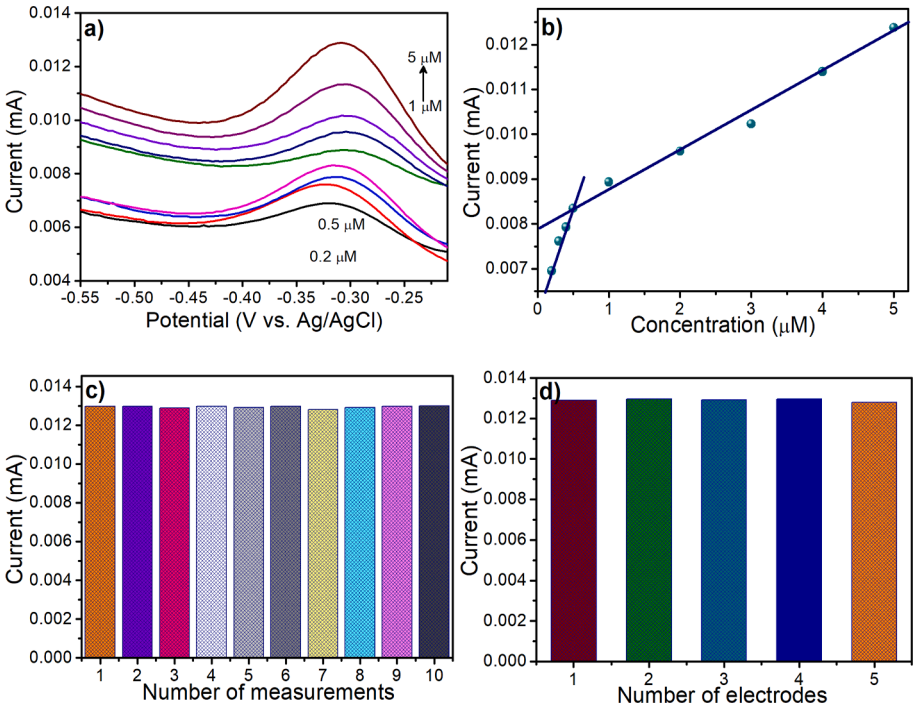


**Fig. 6.** A) dpv profile of znco$_2$O$_4$@MOF/CPE with varied concentrations of glucose (0.2 – 5 μM, pH≈10), b) calibration plot of peak current vs. concentration in $NH_3$-$NH_4Cl$, NaOH (pH≈10), c) repeatability tests with ten successive measurements (5 μM glucose, pH≈10), and d) reproducibility tests with five electrodes maintaining similar experimental conditions (5 μM glucose, pH≈10),.

the system having 0.1 M KCl solution. As increased scan rates showed an increased current response, this shows the fast response kinetics of $ZnCo_2O_4$@MOF/CPE. Fig. 5e) shows the linear calibration equation for change in scan rate. A linear curve of current response vs. square root of the scan rate has followed the equation $I_{pa} = (6.97646e^{-6})\ [\nu^{1/2}] + (-5.56228e^{-6})$, with the regression coefficient $R^2 = 0.998$. Also, the reduction peak response was found to be linear with respect to the square root of the scan rate and followed the linear regression equation y = (−0.00223) $[\nu^{1/2}]$ + (0.00363) with $R^2 = 0.999$. The Electrochemical surface area (ECSA) was calculated using the Randles–Sevcik equation for unmodified CPE and $ZnCo_2O_4$@MOF/CPE.

$$I_{pa} = \left(2.69 \times 10^5\right) n^{3/2} A C D^{1/2} \nu^{1/2}$$

where $I_{pa}$ = response current, $n$ = number of electrons, D = diffusion factor, $\nu$ = scan rate, and C = concentration. The obtained ECSA of unmodified CPE and ZnCo2O4@MOF/CPE was 0.32 $cm^2$, and 0.78 $cm^2$, respectively. The results show that $ZnCo_2O_4$@MOF/CPE possesses high ECSA, which contributes to the higher sensitivity and current response of the present sensor.

For effective electrochemical detection of the intended analytes, the load of electrocatalyst over the surface of the CPE plays an important role. Hence the finely polished CPE surface was loaded with varied quality of the active catalyst (2, 4, 6, 8, and 10 μL) and the corresponding current response was recorded at the scan rate of 100 $mVs^{-1}$ [40,41]. The catalyst loading analysis shows that 8 μL catalyst deposited CPE has shown the best current response among all the other combinations. Hence, the optimized 8 μL concentration of catalyst loading was used as standard in all the further studies for the detection of glucose (Fig. 5f).

The electro-catalytic response of $ZnCo_2O_4$@MOF/CPE was further evaluated using differential pulse voltammetry (DPV), a much more sensitive method for the detection of analytes with enhanced response current. Fig. 6a) displays the DPV response of $ZnCo_2O_4$@MOF/CPE, which was investigated with varied concentrations of glucose [$NH_3$-$NH_4Cl$, and NaOH (pH≈10)]. It is observed that the DPV response has shown linearity in two concentration ranges, i.e. 0.2–0.5 μM range and 1.0–5.0 μM with linear regression coefficient $R^2 = 0.999$ and $R^2 = 0.998$ respectively. Further, stability, selectivity, and reproducibility are important parameters for the real-time application of the sensor. The repeatability of $ZnCo_2O_4$@MOF/CPE with 5 μM of glucose was recorded for ten successive measurements Fig. 6c). The bar plot representation shows ten repeatable readings of $ZnCo_2O_4$@MOF/CPE with a relative standard deviation (RSD) of 2.8 %, which shows that the $ZnCo_2O_4$@-MOF/CPE sensor has good repeatability. The reproducibility tests were conducted with five $ZnCo_2O_4$@MOF/CPE electrodes maintaining all the experimental conditions the same. Fig. 6d) shows the respective bar plot of five electrodes – Better retention of the current response was noticed in all the cases with an RSD of 3.2 %, endorsing that the present sensor shows good reproducibility. The effect of pH and the supporting electrolytes used in the detection of glucose were evaluated. To adjust the pH = 5.0 and 6.0 (0.2 M) NaOAc and (0.2 M) HOAc electrolytes were used. pH = 7.0 and 8.0 (0.2 M) $Na_2HPO_4$ and (0.2 M) $NaH_2PO_4$ were used and 0.2 M $NH_3$ and 0.2 M $NH_4Cl$, and NaOH were used to adjust the pH of the solution to 9.0 and 12.0. The current response of the sensor was maximum at pH = 10. As shown in Fig. 6c, the peak current enhanced slowly from a pH of 5.0 to 10.0, and consequently declined. The improved peak current observed at pH 10 was due to the participation and rapid electron movement to the electrode. Also, the isoelectric point of zinc in its oxide form is IEP = 9.5, hence under alkaline conditions the surface of $ZnCo_2O_4$@MOF is strongly negatively charged repelling the common interferents during glucose detection providing high selectivity of the sensor towards the detection of glucose [42]. Therefore, pH 10 is preferred to be the optimum pH, and $NH_4OH$ – $NH_4Cl$, NaOH is used as a supporting electrolyte during the electrochemical detection of glucose in the present investigation.

*EIS analysis*

To validate the behavior of charge transfer at $ZnCo_2O_4$@MOF/CPE and bare CPE electrodes, the EIS analysis was carried out at frequencies ranging from 0.01 Hz to 100 kHz in KCl solution. The straight line for $ZnCo_2O_4$@MOF/CPE was observed at lower frequencies which were

**Table 1**
Equivalent circuit parameters obtained from EIS for CPE and $ZnCo_2O_4$@MOF/CPE.

| Electrode | Rs (Ω) | Cdl (μF) | Rct (Ω) |
|---|---|---|---|
| CPE | 2.14 | 11.78 | 12.8 |
| $ZnCo_2O_4$@MOF/CPE | 1.52 | 78.25 | 6.75 |

almost vertical and approached the (−Z'') imaginary axis. Low ionic diffusion resistance was observed between the modified electrode material and the electrolyte. Charge transfer resistance is indicated by the semicircle in the higher frequency range indicating the diffusion of electrolyte at the electrolyte–electrode interface. Referring to the Nyquist waveforms, the Rct values of the synthesized materials are in the following sequence: $ZnCo_2O_4$@MOF/CPE (6.75 Ω) < CPE (12.8 Ω). The better electron transfer rate and improved surface area were also evident from the decreased charge transfer resistance for $ZnCo_2O_4$@MOF/CPE (6.75 Ω) compared to CPE (12.8 Ω) Table 1, and the corresponding equivalent circuit is shown in the inset of Fig. 7a). The double layer capacitance of CPE (11.78 μF) and $ZnCo_2O_4$@MOF/CPE (78.25 μF) clearly shows improved electrochemical active surface area of the modified electrode. All these features enhance the electrical conductivity, which can probably improve sensitivity and response time. This proves that the $ZnCo_2O_4$@MOF/CPE sensor is an ideal choice to accelerate electron transfer and better glucose detection.

*Amperometric analysis*

Amperometric experiments were carried out to assess the electrochemical performance of $ZnCo_2O_4$@MOF/CPE at −0.4 V, −0.45 V, −0.5 V, and −0.55 V potentials in the 1 M KCl solution with NaOH. To further carry out the amperometric measurements and to avoid interference effects, −0.4 V was selected to be the working potential. In glucose oxidation, a greater anodic current was observed for $ZnCo_2O_4$@MOF/CPE at a potential 0.4 V. The amperometric responses with sequential step addition of glucose (0.1 – 100 μM) at $ZnCo_2O_4$@MOF/CPE were recorded and found to be linear with concentration. After successive addition of glucose, the current response increased in a stepwise manner in less than 1 s on average. This was influenced by the conductive nature of $ZnCo_2O_4$@MOF/CPE, its rapid response, and high selectivity towards glucose. The steady-state condition was attained in not more than 2 s. This was due to the phenomena of quick adsorption and diffusion of glucose molecules on the surface of $ZnCo_2O_4$@MOF/CPE. Thus, the fabricated electrode exhibited a rapid response time intended for glucose detection.

The calibration plot of the amperometric response concerning the change in the concentration of the analyte glucose is presented in Fig. 8b). The plot follows the linear regression equation $i_a$=(0.04646) [Glucose] + 0.03338 with $R^2$ = 0.9984. The sensor has shown an excellent limit of detection (LOD) of 0.0248 μM (24.8 nM) and the limit of quantification was found to be 0.075 μM (75 nM) (Fig. 8c). For the practical application of a sensor, it must be interferrant-free, there are common interferrants like Ascorbic acid (AA = 5 μM), Uric acid (UA = 5 μM), Dopamine (DA = 5 μM), and Urea (Ur = 5 μM). To check the interference of all these molecules during the determination of glucose, their concentrations were maintained tenfold greater than glucose. As obvious, no significant current response was noticed for any of the molecules, this demonstrates that $ZnCo_2O_4$@MOF/CPE is an interferent-free highly selective glucose sensor (Fig. 8d). Additionally, the persistent nature of $ZnCo_2O_4$@MOF/CPE was examined with the addition of 1 μM of glucose for 30 days. The bar plot of the amperometric peak current response recorded at the successive 5 days gap for the same electrode recorded over 30 days showed an insignificant loss in the activity and could retain 97.3 % of its initial current response even after 30 days of storage, this shows a high storage stability of the present sensor. The mechanism involving the cobalt reduction–oxidation system for the non-enzymatic glucose detection has been pictorially given in Fig. 8e), where the glucose undergoes oxidation to glucanolactone and on the other hand cobalt undergoes reduction to $Co^{2+}$.

*Real sample analysis*

The robustness of the fabricated sensor ($ZnCo_2O_4$@MOF/CPE) for the determination of glucose in the human serum samples was tested by the standard addition method. 0.1 ml of human serum was injected into 5 ml of 0.1 M NaOH. The blood serum samples were spiked with a known quantity of glucose. The relative standard deviations (RSD) were investigated using the standard addition method, and the results are summarized in Table 2. The recovery ranged between 99.6 and 101.6 % for glucose. Therefore, it can be concluded that the $ZnCo_2O_4$@MOF/CPE sensor is promising for monitoring glucose in real serum samples. Further, to compare the competitiveness of the present sensor a table comparing the results of the present sensor with that reported in the literature was given in Table 3.

## Conclusions

The interest in designing and optimizing MOF template-mediated $ZnCo_2O_4$/CPE electrodes was inspired by the emerging applications of electrochemical sensors in personal health monitoring devices. Here, $ZnCo_2O_4$@MOF/CPE was fabricated for non-enzymatic glucose sensing. The effective synthesis of $ZnCo_2O_4$@MOF/CPE was confirmed by SEM, TEM, XRD, FTIR, and XPS analysis. Amperometry was employed to detect the glucose concentration and measure its current response. Voltametric measurements were done to quantify the output of current. The $ZnCo_2O_4$@MOF/CPE sensor exhibited a lower detection limit of 24.8 nM. In addition, it showed a wide detection range of 0.1 μM – 100 μM. This electrode showed improved reproducibility and recovery rates. The performance of $ZnCo_2O_4$@MOF/CPE was strongly influenced by the synergism between Zn, Co, and O prepared via MOF template mediated process leading to greater selectivity and stability. Thus, the fabricated

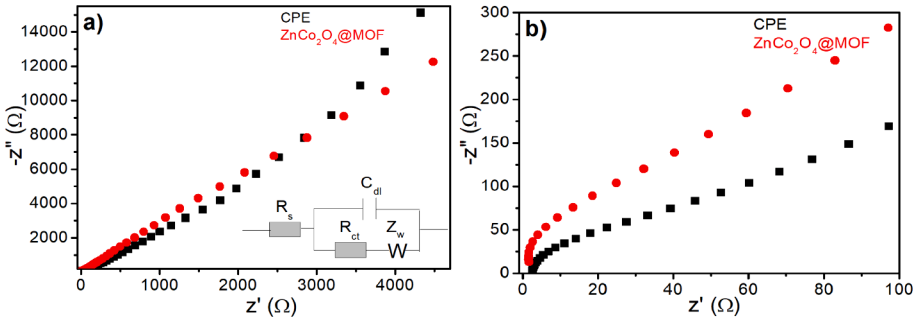


**Fig. 7.** A) nyquist plots of cpe, and znco$_2$O$_4$@MOF/CPE illustrated the appearance of the Warburg coefficient, indicating the charge diffusion within the electrode system; Inset: The Randle's circuit used to fit the data. b) Enlarged view of Nyquist plot at higher frequency region.

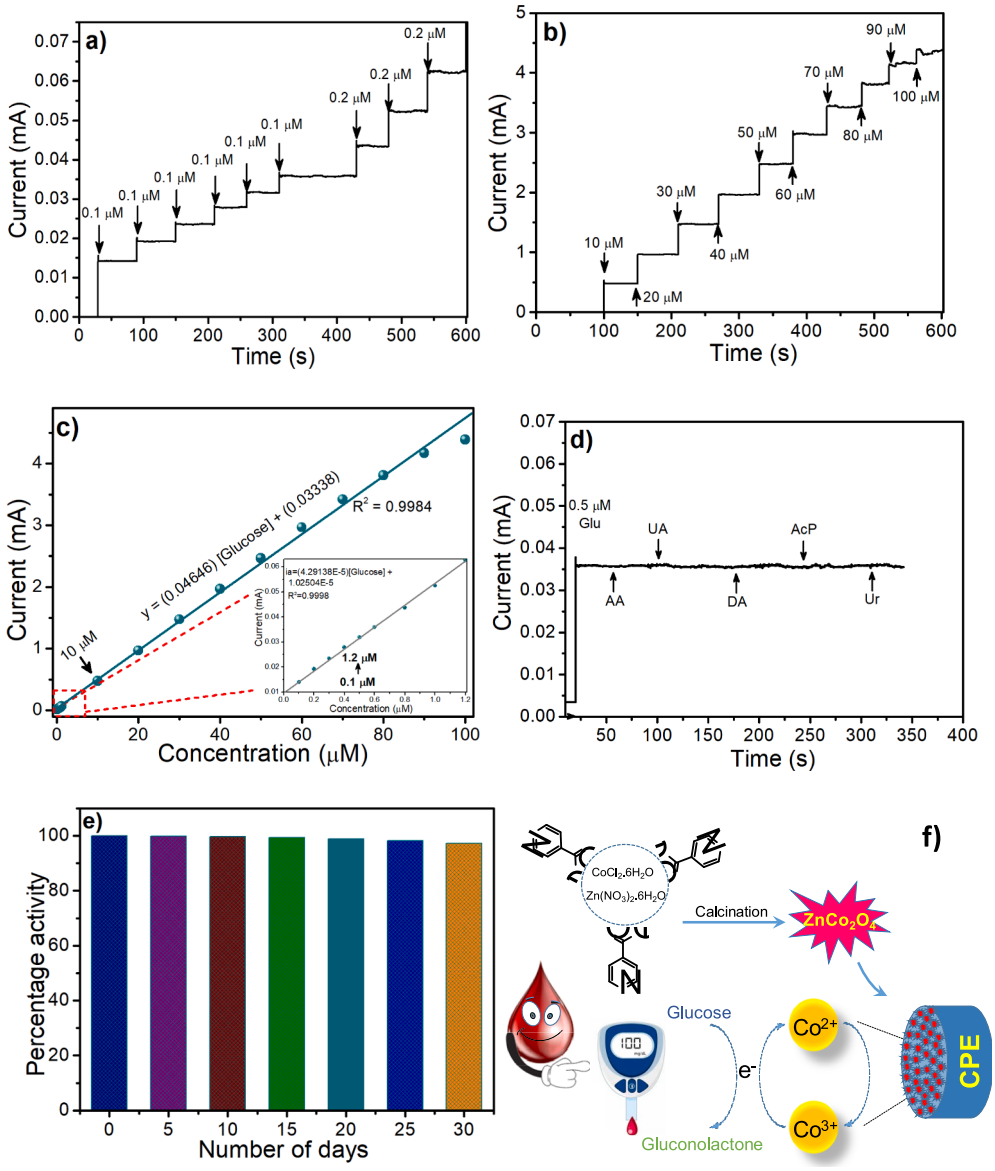


**Fig. 8.** A) Amperometric current response at $ZnCo_2O_4$@MOF/CPE for successive glucose addition (Glucose 0.1–1.2 μM, pH≈10, KCl = 0.1 M), and b) Glucose 10 – 100 μM, pH≈10, KCl = 0.1 M; c) Calibration plot of current response with the concentration of glucose (0.1 – 100 μM, $R^2 = 0.9984$), c) Selectivity study for the sensor in presence of (AA = 5 μM, UA = 5 μM, DA = 5 μM, AcP = 5 μM, and Ur = 5 μM), and e) Storage stability study of the sensor (percentage activity retention v/s time) (Electrode preserved in 0.1 M KCl solution). f) Pictorial representation of the mechanism of glucose detection at $ZnCo_2O_4$@MOF/CPE.

**Table 2**
Recovery data for determination of glucose in human blood serum samples under optimized conditions at $ZnCo_2O_4$@MOF/CPE.

| Sample | Spiked (μM) | Found (μM) | Recovery (%) | RSD (%) (n = 3) |
|---|---|---|---|---|
| | Glucose | Glucose | Glucose | Glucose |
| **Human serum** | 5 | 4.98 | 99.6 | 0.4 |
| | 10 | 10.1 | 101 | 1.0 |
| | 25 | 25.3 | 101.2 | 1.2 |
| | 50 | 50.8 | 101.6 | 0.6 |
| | 100 | 99.9 | 99.9 | 0.65 |

electrode is particularly useful in the clinical and biomedical monitoring of glucose.

## CRediT authorship contribution statement

**K. Divyarani:** Writing – original draft, Formal analysis, Data curation. **S. Sreenivasa:** Formal analysis, Data curation. **Sandeep Kumar:** Formal analysis, Data curation. **Anjana Vinod:** Investigation, Formal analysis. **Fahd Alharethy:** Investigation, Formal analysis, Data curation. **Byong-Hun Jeon:** Validation, Methodology, Funding acquisition, Formal analysis, Data curation. **V.S. Anusuya Devi:** . **Praveen Martis:** Writing – review & editing, Formal analysis, Data curation. **L. Parashuram:** .

## Declaration of competing interest

The authors declare that they have no known competing financial interests or personal relationships that could have appeared to influence the work reported in this paper.

## Data availability

Data will be made available on request.

**Table 3**
Comparison of performance of non-enzymatic electrochemical sensors with other sensors found in the literature for the detection of glucose.

| Sl. No. | Electrode | Applied potential (V) | sensitivity (μA $mM^{-1}cm^{-2}$) | Linear range (mM) | Electrolyte | Detection limit (μM) | Response time (s) | Ref. |
|---|---|---|---|---|---|---|---|---|
| 1. | Ni-BDC-$NH_2$ | 0–0.7 | 308<br>727<br>102.80 | 0.1 to 1.4<br>0.067–1.373<br>2 to 8 | 0.1 M NaOH | 3.82 | 5.4 | [43] |
| 2. | Cu-MOF/CPE | 0.45 | – | 0.005–10.95 | 0.1 M NaOH | 0.11 | 0.5 | [44] |
| 3. | Co-MOF | 0.4 | 169 | 0.005–0.9 | 0.01 M NaOH | 1.6 | 7 | [45] |
| 4. | $NiCo_2O_4$ nanobelt | 0.45 | 5000 | 0.9–67.2 | 0.5 M NaOH | 0.9 | 4 | [46] |
| 5. | Ni-BDC MOF | 0.6 to 1.0 | 635.9 | 0.01 to 0.8 | 0.1 M NaOH | 6.68 | <5 | [47] |
| 6. | $Co_3O_4$ | 0.55 | 254.21 | 0.001 to 2 | 0.1 M NaOH | – | – | [48] |
| 7. | Bimetallic Cu@Ni organic framework microsphere | 0.54 | 496 | 0–5 | 0.1 M NaOH | 0.4 | – | [49] |
| 8. | Cu(II)/rGO/SPCE | 0.50 | 172 | 0.10 to 12.5 | 0.1 M NaOH | 65 | – | [50] |
| 9 | $ZnCo_2O_4$@MOF | 0.4 | – | 0.1 to 100 | 0.1 M KCl + 0.1 NaOH | 24.8 nM | <2 | Our work |

## Acknowledgments

The authors are thankful to the Management of Nitte Meenakshi Institute of Technology, Bangalore. Department of Chemistry, Tumkur University Tumakuru. The authors extend their thanks to the Researchers Supporting Project (RSP2024R160), King Saud University (Riyadh, Saudi Arabia), and Korea Institute of Energy Technology Evaluation and Planning (KETEP) grant by the Ministry of Trade, Industry and Energy (MOTIE) of South Korean Government (No. 20206410100040) for their continuous support for the successful completion of the present work.

## References

[1] K. Bannier, M. Lichtenauer, M. Franz, M. Fritzenwanger, B. Kabisch, H.R. Figulla, R. Pfeifer, C. Jung, Impact of diabetes mellitus and its complications: survival and quality-of-life in critically ill patients, J. Diabetes Complications. 29 (2015) 1130–1135, https://doi.org/10.1016/j.jdiacomp.2015.08.010.
[2] N. Cheung, T.Y. Wong, Diabetic retinopathy and systemic vascular complications, Prog. Retin. Eye Res. 27 (2008) 161–176, https://doi.org/10.1016/j.preteyeres.2007.12.001.
[3] Z. Mian, K.L. Hermayer, A. Jenkins, Continuous glucose monitoring: review of an innovation in diabetes management, Am. J. Med. Sci. 358 (2019) 332–339, https://doi.org/10.1016/j.amjms.2019.07.003.
[4] G. Freckmann, J.H. Nichols, R. Hinzmann, D.C. Klonoff, Y. Ju, P. Diem, K. Makris, R.J. Slingerland, Standardization process of continuous glucose monitoring: traceability and performance, Clin. Chim. Acta. 515 (2021) 5–12, https://doi.org/10.1016/j.cca.2020.12.025.
[5] J. Chen, J. Ge, L. Zhang, Z. Li, L. Qu, Poly(styrene sulfonate) and Pt bifunctionalized graphene nanosheets as an artificial enzyme to construct a colorimetric chemosensor for highly sensitive glucose detection, Sensors Actuators, B Chem. 233 (2016) 438–444, https://doi.org/10.1016/j.snb.2016.04.118.
[6] K. Mitsubayashi, T. Ohgoshi, T. Okamoto, Y. Wakabayashi, M. Kozuka, K. Miyajima, H. Saito, H. Kudo, Tonometric biosensor with a differential pressure sensor for chemo-mechanical measurement of glucose, Biosens. Bioelectron. 24 (2009) 1518–1521, https://doi.org/10.1016/j.bios.2008.08.014.
[7] J.T. Suri, D.B. Cordes, F.E. Cappuccio, R.A. Wessling, B. Singaram, Continuous glucose sensing with a fluorescent thin-film hydrogel, Angew Chemie. 115 (2003) 6037–6039, https://doi.org/10.1002/ange.200352405.
[8] W. Meng, Y. Wen, L. Dai, Z. He, L. Wang, A novel electrochemical sensor for glucose detection based on Ag@ZIF-67 nanocomposite, Sensors Actuators, B Chem. 260 (2018) 852–860, https://doi.org/10.1016/j.snb.2018.01.109.
[9] J. Mohapatra, B. Ananthoju, V. Nair, A. Mitra, D. Bahadur, N.V. Medhekar, M. Aslam, Enzymatic and non-enzymatic electrochemical glucose sensor based on carbon nano-onions, Appl. Surf. Sci. 442 (2018) 332–341, https://doi.org/10.1016/j.apsusc.2018.02.124.
[10] M.S. Gangadharappa, M.S. Raghu, S. Kumar, L. Parashuram, V.U. Kumar, Elaeocarpus ganitrus structured mesoporous hybrid $mn^{3+/4+}$ loaded zirconia self assembly as a versatile amperometric probe for the electrochemical detection of nitrite, ChemistrySelect. 6 (2021), https://doi.org/10.1002/slct.202004543.
[11] L. Parashuram, S. Sreenivasa, S. Akshatha, V. Udayakumar, S. Sandeep kumar, A non-enzymatic electrochemical sensor based on ZrO2: Cu(I) nanosphere modified carbon paste electrode for electro-catalytic oxidative detection of glucose in raw Citrus aurantium var. sinensis, Food Chem. 300 (2019) 125178, https://doi.org/10.1016/j.foodchem.2019.125178.
[12] S. Prasanna Kumar, L. Parashuram, D.P. Suhas, P. Krishnaiah, Carboxylated graphene-alcohol oxidase thin films modified graphite electrode as an electrochemical sensor for electro-catalytic detection of ethanol, Mater. Sci. Energy Technol. (2019), https://doi.org/10.1016/j.mset.2019.10.009.
[13] A. Alsulami, Y.K. Kumarswamy, M.K. Prashanth, S. Hamzada, P. Lakshminarayana, C.B. Pradeep Kumar, B.H. Jeon, M.S. Raghu, Fabrication of FeVO4/RGO nanocomposite: an amperometric probe for sensitive detection of methyl parathion in green beans and solar light-induced degradation, ACS Omega. 7 (2022) 45239–45252, https://doi.org/10.1021/acsomega.2c05729.
[14] P. Zhang, J. Li, J. Feng, Y. Wang, A. Xu, T. Chen, L. Zhao, F. Dang, X. Zhang, H. Wang, MOF-template derived hollow CeO2/Co3O4 polyhedrons with efficient cathode catalytic capability in Li-O2 batteries, Chinese Chem. Lett. 32 (2021) 2438–2442, https://doi.org/10.1016/j.cclet.2021.02.010.
[15] Y. Zhang, J. Zhou, X. Chen, Q. Feng, W. Cai, MOF-derived C-doped ZnO composites for enhanced photocatalytic performance under visible light, J. Alloys Compd. 777 (2019) 109–118, https://doi.org/10.1016/j.jallcom.2018.10.383.
[16] R. Guo, X. Hou, C. Shi, W. Zhang, Y. Zhou, MOF-derived Co3O4 hierarchical porous structure for enhanced acetone sensing performance with high sensitivity and low detection limit, Sensors Actuators b. Chem. 376 (2023) 132973, https://doi.org/10.1016/j.snb.2022.132973.
[17] L. Cheng, Y. He, M. Gong, X. He, Z. Ning, H. Yu, Z. Jiao, MOF-derived synthesis of Co3O4 nanospheres with rich oxygen vacancies for long-term stable and highly selective n-butanol sensing performance, J. Alloys Compd. 857 (2021) 158205, https://doi.org/10.1016/j.jallcom.2020.158205.
[18] Z. Lu, J. Zhong, Y. Zhang, M. Sun, P. Zou, H. Du, X. Wang, H. Rao, Y. Wang, MOF-derived Co3O4/FeCo2O4 incorporated porous biomass carbon : Simultaneous electrochemical determination of dopamine, acetaminophen and xanthine, J. Alloys Compd. 858 (2021) 157701, https://doi.org/10.1016/j.jallcom.2020.157701.
[19] M. Caglar, S. Ruzgar, Influence of the deposition temperature on the physical properties of high electron mobility ZnO films by sol-gel process, J. Alloys Compd. 644 (2015) 101–105, https://doi.org/10.1016/j.jallcom.2015.04.167.
[20] V. Adimule, P. Lakshminarayana, C. Bathula, B.H. Jeon, Insight into electro chemical and dielectric properties of flower shaped samarium embedded Y2O3@SeO2 nanocomposites for H2O2 sensor applications, Mater. Today Commun. 38 (2024) 108163, https://doi.org/10.1016/j.mtcomm.2024.108163.
[21] V. Adimule, K. Sharma, P. Lakshminarayana, S. Rajendrachari, R. Keri, F. A. Alharthi, Fabrication of carbon nanospheres functionalized Sm2O3/Co3O4 novel hybrid nanocomposites for selective and sensitive amperometric detection of hydrogen peroxideYusri, Ahman, J Appl Electrochem. 54 (2024) 323–340.
[22] V. Consonni, A.M. Lord, Polarity in ZnO nanowires: a critical issue for piezotronic and piezoelectric devices, Nano Energy. 83 (2021) 105789, https://doi.org/10.1016/j.nanoen.2021.105789.
[23] Y. Adachi, N. Saito, I. Sakaguchi, T.T. Suzuki, Polarity dependent gas sensing properties of ZnO thin films, Thin Solid Films. 685 (2019) 238–244, https://doi.org/10.1016/j.tsf.2019.06.023.
[24] L. Dai, M. Liu, Y. Song, J. Liu, F. Wang, Mn3O4-decorated Co3O4 nanoparticles supported on graphene oxide: Dual electrocatalyst system for oxygen reduction reaction in alkaline medium, Nano Energy. 27 (2016) 185–195, https://doi.org/10.1016/j.nanoen.2016.07.007.
[25] J. Ma, H. Wei, Y. Liu, X. Ren, Y. Li, F. Wang, X. Han, E. Xu, X. Cao, G. Wang, F. Ren, S. Wei, Application of Co3O4-based materials in electrocatalytic hydrogen evolution reaction: A review, Int. J. Hydrogen Energy. 45 (2020) 21205–21220, https://doi.org/10.1016/j.ijhydene.2020.05.280.
[26] N. Bhuvanendran, M.G. Choi, D. Kim, S.Y. Lee, Improved trifunctional electrocatalytic performance of integrated Co3O4 spinel oxide morphologies with abundant oxygen vacancies for oxygen reduction and water-splitting reactions, J. Alloys Compd. 935 (2023) 168079, https://doi.org/10.1016/j.jallcom.2022.168079.

[27] G. Rajeshkhanna, E. Umeshbabu, G. Ranga Rao, Charge storage, electrocatalytic and sensing activities of nest-like nanostructured Co3O4, J. Colloid Interface Sci. 487 (2017) 20–30, https://doi.org/10.1016/j.jcis.2016.10.011.
[28] M. Pan, D. Feng, Y. Ouyang, D. Yang, X. Yu, L. Xu, I. Willner, MOF-templated synthesis of cobalt-doped zinc oxide superparticles for detection of the 3-hydroxy-2-butanone microbial biomarker, Sensors Actuators B . Chem. 358 (2022) 131482 Contents. https://doi.org/10.1016/j.snb.2022.131482.
[29] D. Hoon, T. Thi, T. Nguyen, S.T. Navale, L. Ho, T. Nguyen, Y.T. Dang, N. Xuan, D. Mai, T. Bach, J. Kim, T. Le, H. Doan, S. Sub, H. Woo, Novel amine-functionalized zinc-based metal-organic framework for low-temperature chemiresistive hydrogen sensing, Sensors Actuators b. Chem. 368 (2022) 132120, https://doi.org/10.1016/j.snb.2022.132120.
[30] M. Ataei Kachouei, S. Shahrokhian, M. Ezzati, Bimetallic CoZn-MOFs easily derived from CoZn-LDHs, as a suitable platform in fabrication of a non-enzymatic electrochemical sensor for detecting glucose in human fluids, Sensors Actuators B Chem. 344 (2021) 130254, https://doi.org/10.1016/j.snb.2021.130254.
[31] M. Silambarasan, P.S. Ramesh, D. Geetha, K. Ravikumar, H.E. Ali, H. Algarni, P. Soundhirarajan, K.V. Chandekar, M. Shkir, A facile preparation of zinc cobaltite (ZnCo2O4) nanostructures for promising supercapacitor applications, J. Inorg. Organomet. Polym. Mater. 31 (2021) 3905–3920, https://doi.org/10.1007/s10904-021-02077-z.
[32] L. Xu, Y. Zhao, J. Lian, Y. Xu, J. Bao, J. Qiu, L. Xu, H. Xu, M. Hua, H. Li, Morphology controlled preparation of ZnCo2O4 nanostructures for asymmetric supercapacitor with ultrahigh energy density, Energy. 123 (2017) 296–304, https://doi.org/10.1016/j.energy.2017.02.018.
[33] R. Naik, S.C. Prashantha, H. Nagabhushana, Y.V. Naik, K.M. Girish, H. B. Premkumar, Photoluminescent and thermoluminescent properties of low temperature synthesized Nd3+ doped Mg2SiO4 nanophosphors for display and dosimetry applications, Optik (stuttg). 180 (2019) 8–19, https://doi.org/10.1016/j.ijleo.2018.11.069.
[34] S. Chakrabarty, A. Mukherjee, W.N. Su, S. Basu, Improved bi-functional ORR and OER catalytic activity of reduced graphene oxide supported ZnCo2O4 microsphere, Int. J. Hydrogen Energy. 44 (2019) 1565–1578, https://doi.org/10.1016/j.ijhydene.2018.11.163.
[35] S. Balasurya, M.K. Okla, M.A. Abdel-maksoud, S.R. Ahamad, F. Almasoud, H. AbdElgawad, A.M. Thomas, L.L. Raju, S. Sudheer Khan, Fabrication of Ag-ZnCo2O4 framework on chitosan matrix for discriminative dual mode detection of S2- ions and cysteine, and cyto-toxicological evaluation, J. Mol. Liq. 347 (2022) 118356, https://doi.org/10.1016/j.molliq.2021.118356.
[36] R. Naik, S.C. Prashantha, H. Nagabhushana, S.C. Sharma, H.P. Nagaswarupa, K. S. Anantharaju, B.M. Nagabhushana, H.B. Premkumar, K.M. Girish, A single phase, red emissive Mg2SiO4:Sm3+ nanophosphor prepared via rapid propellant combustion route, Spectrochim. Acta - Part A Mol. Biomol. Spectrosc. 140 (2015) 516–523, https://doi.org/10.1016/j.saa.2015.01.011.
[37] G. Ramakrishna, R. Naik, H. Nagabhushana, R.B. Basavaraj, S.C. Prashantha, S. C. Sharma, K.S. Anantharaju, White light emission and energy transfer (Dy3+ → Eu3+) in combustion synthesized YSO: Dy3+, Eu3+ nanophosphors, Optik (stuttg). 127 (2016) 2939–2945, https://doi.org/10.1016/j.ijleo.2015.11.234.
[38] S. Ashwini, S.C. Prashantha, R. Naik, Y.V. Naik, H. Nagabhushana, D. M. Jnaneshwara, Photoluminescence of a novel green emitting Bi2O3:Tb3+ nanophosphors for display, thermal sensor and visualisation of latent fingerprints, Optik (stuttg). 192 (2019) 162956, https://doi.org/10.1016/j.ijleo.2019.162956.
[39] V.V. Shanbhag, S.C. Prashantha, T.R.S. Shekhar, H. Nagabhushana, R. Naik, K. M. Girish, S. Ashwini, D. Rangappa, D.S. Prasanna, Enhanced photoluminescence of SiO2 coated CaTiO3:Dy3+, Li+ nanophosphors for white light emitting diodes, Ceram. Int. 47 (2021) 10346–10354, https://doi.org/10.1016/j.ceramint.2020.11.077.
[40] M. Maheshwaran, K.K. Satheesh Kumar, DFT and electrochemical determination of Hg2+ and Pb2+ in water using polyaniline–quinoxaline composite modified GCE electrode, J. Mol. Liq. 398 (2024) 124317, https://doi.org/10.1016/j.molliq.2024.124317.
[41] M. Maheshwaran, G. Sivaraman, K.K.S. Kumar, An electrochemical voltammetric response of Hg2+ and Pb2+ ions using polyaniline-benzothiazole composite modified GCE electrode: Synthesis, characterization and quantum chemical calculation, Microchem. J. 197 (2024) 109865, https://doi.org/10.1016/j.microc.2023.109865.
[42] A. Degen, M. Kosec, Effect of pH and impurities on the surface charge of zinc oxide in aqueous solution, J. Eur. Ceram. Soc. 20 (2000) 667–673, https://doi.org/10.1016/S0955-2219(99)00203-4.
[43] A.D. Daud, H.N. Lim, I. Ibrahim, N.A. Endot, N.S.K. Gowthaman, Z.T. Jiang, K. E. Cordova, An effective metal-organic framework-based electrochemical non-enzymatic glucose sensor, J. Electroanal. Chem. 921 (2022) 116676, https://doi.org/10.1016/j.jelechem.2022.116676.
[44] L. Wu, Z.W. Lu, Y. Ma, J.J. Zhang, G.Q. Mo, H.J. Du, J.S. Ye, Cu(II) Metal-Organic Framework Encapsulated in Carbon Paste Electrode for High-Performance Non-Enzymatic Glucose Sensing, Chinese, J. Anal. Chem. 48 (2020) e20038–e20046, https://doi.org/10.1016/S1872-2040(20)60006-8.
[45] L. Zhang, N. Wang, P. Cao, M. Lin, L. Xu, H. Ma, Electrochemical non-enzymatic glucose sensor using ionic liquid incorporated cobalt-based metal-organic framework, Microchem. J. 159 (2020) 105343, https://doi.org/10.1016/j.microc.2020.105343.
[46] J. Zhang, Y. Sun, X. Li, J. Xu, Fabrication of NiCo2O4 nanobelt by a chemical co-precipitation method for non-enzymatic glucose electrochemical sensor application, J. Alloys Compd. 831 (2020) 154796, https://doi.org/10.1016/j.jallcom.2020.154796.
[47] G. Gumilar, Y.V. Kaneti, J. Henzie, S. Chatterjee, J. Na, B. Yuliarto, N. Nugraha, A. Patah, A. Bhaumik, Y. Yamauchi, General synthesis of hierarchical sheet/plate-like M-BDC (M = Cu, Mn, Ni, and Zr) metal-organic frameworks for electrochemical non-enzymatic glucose sensing, Chem. Sci. 11 (2020) 3644–3655, https://doi.org/10.1039/c9sc05636j.
[48] C. Han, L. Nie, X. Han, X. Zhuang, J. Zhang, Y. Rui, W. Meng, A good-performance glucose sensor fabricated via rationally designing a new cobalt-metal-organic framework precursor, New J. Chem. 44 (2020) 14896–14905, https://doi.org/10.1039/d0nj03403g.
[49] S. Eun Kim, A. Muthurasu, Metal-organic framework–assisted bimetallic Ni@Cu microsphere for enzyme-free electrochemical sensing of glucose, J. Electroanal. Chem. 873 (2020) 114356, https://doi.org/10.1016/j.jelechem.2020.114356.
[50] S. Phetsang, P. Kidkhunthod, N. Chanlek, J. Jakmunee, P. Mungkornasawakul, K. Ounnunkad, Copper/reduced graphene oxide film modified electrode for non-enzymatic glucose sensing application, Sci. Rep. 11 (2021) 1–13, https://doi.org/10.1038/s41598-021-88747-x.